

## Research Article

# Ductility and Ultimate Capacity of Prestressed Steel Reinforced Concrete Beams

**Chengquan Wang, Yonggang Shen, Runfang Yang, and Zuolin Wen**

*Department of Civil Engineering, Zhejiang University, Hangzhou 310058, China*

Correspondence should be addressed to Yonggang Shen; sygdesign@zju.edu.cn

Received 17 October 2016; Revised 9 February 2017; Accepted 28 February 2017; Published 28 March 2017

Academic Editor: R. Emre Erkmen

Copyright © 2017 Chengquan Wang et al. This is an open access article distributed under the Creative Commons Attribution License, which permits unrestricted use, distribution, and reproduction in any medium, provided the original work is properly cited.

Nonlinear numerical analysis of the structural behaviour of prestressed steel reinforced concrete (PSRC) beams was carried out by using finite element analysis software ABAQUS. By comparing the load-deformation curves, the rationality and reliability of the finite element model have been confirmed; moreover, the changes of the beam stiffness and stress in the forcing process and the ultimate bearing capacity of the beam were analyzed. Based on the model, the effect of prestressed force, and H-steel to the stiffness, the ultimate bearing capacity and ductility of beam were also analyzed.

## 1. Introduction

Nowadays, the prestressed concrete structural components with their excellent performance have a wide range of applications in housing construction, bridges, water, and other civil engineering projects [1–5]. Prestressed steel reinforced concrete (PSRC) structure is a new type of structure which improves the mechanical properties with the application of the prestressed technology. PSRC structure has double advantages of steel reinforced concrete (SRC) structure and prestressed concrete structure; the built-in steel can improve the structural load carrying capacity and seismic performance, while the application of prestressed technology can ameliorate the performance of the structure under service load conditions (such as crack control and deformation control), so PSRC structure is easy to achieve large span, heavy load structure [2, 6, 7].

As a result, it was quite necessary to make in-depth analysis on the static and dynamic characteristics of PSRC beam. A large number of engineering practices show that the finite element method was a quite effective method in numerical analysis methods [8]. In this paper, analysis of the structural behaviour of PSRC beams was carried out using the ABAQUS.

## 2. Finite Element Simulation

**2.1. Introduction of the Finite Element Model.** In order to verify the effectiveness and rationality of finite element analysis, first of all, test components in the papers of Wenzhong et al. [9] were used as research objects, and a two-span PSRC beam finite element model was established. The beam cross-section is shown in Figure 1, and the designed strength grade of concrete was C40; the prestressing steel was  $\phi^s15$  steel strand, the tensile strength of which was  $f_{ptk} = 1860 \text{ N/mm}^2$ , the inner diameter of corrugated duct was 50 mm, and initial tensile stress  $\sigma_{con} = 0.75f_{ptk}$ ; bonded tendons were used; the material grade of H-steel ( $H \times B \times t_1 \times t_2 = 100 \text{ mm} \times 100 \text{ mm} \times 6 \text{ mm} \times 8 \text{ mm}$ ) was Q235, and H-steel was symmetrically arranged in beam cross-section; stirrups are  $\phi12@100$  and material was HPB235; the tendon profile is shown in Figure 2.

**2.2. Prestressing Effect Simulation.** The equivalent load method and physical reinforcement method are two kinds of prestressing simulation methods; the equivalent load method is that the prestressed is converted to an equivalent load applied to the structure. But this method uses simplified assumptions, which cannot simulate the prestressed spatial effect on the structure and cannot simulate the complex

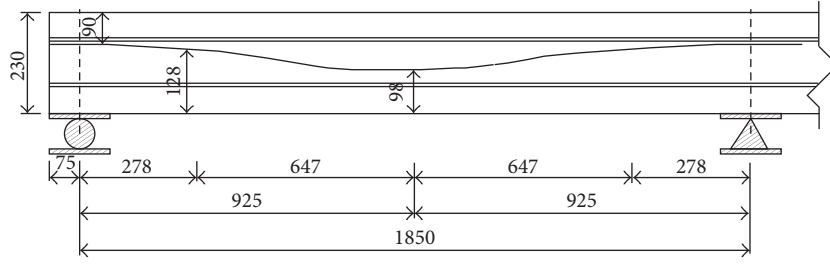


FIGURE 1: Tendon profile.

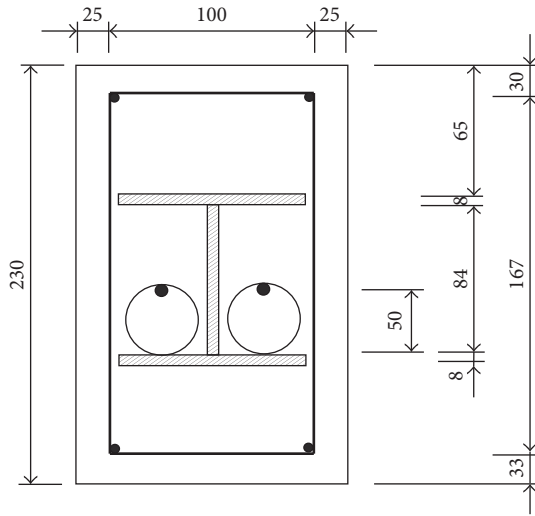


FIGURE 2: Cross-section of PSRC beam.

force structure; physical reinforcement method contains entity segmentation method, the node coupling method, and constraint equation method, in which prestressing is simulated by cooling and initial strain method. Cooling method is relatively simple and can simulate stress losses; initial strain method usually ignores the prestress loss; otherwise, each of the real constants is not equal, which is a larger workload.

In this paper, cooling method was used to simulate the prestressing effect [9]. At first, we set an initial temperature value and a temperature drop value for reinforced unit to make reinforced unit generate contraction deformation; this initial strain will let the reinforced steel pretensioned as prestress in the finite element model. Steel temperature drop value was calculated as follows:

$$\Delta T = \frac{\sigma}{E\alpha}, \quad (1)$$

where  $\Delta T$  is the value of temperature drop;  $E$  is the elastic modulus of prestressing steel;  $\alpha$  is the linear expansion coefficient;  $\sigma$  is the effective prestressing values.

**2.3. The Connection between Steel and Concrete.** In this paper, the bond relationship between steel and concrete is simulated through embedded region method in ABAQUS. Embedded

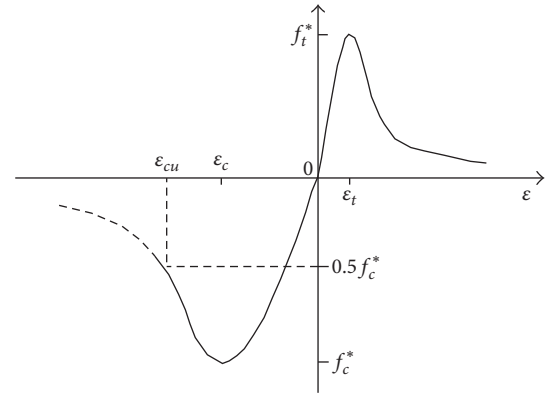


FIGURE 3: Concrete constitutive relationship.

region method is usually designated to deal with one or a group of cells located in other units arrested problems; the method can handle tendons and steel mesh [10]. The interaction between cracked concrete and reinforcement that is known as “bond-slip” is indirectly included by modifying the postpeak behaviour of concrete which is modeled by “tension stiffening” effect for concrete in tension [11].

**2.4. Material Properties.** In this article, the concrete constitutive relationship is referenced from Chinese Code for Design of Concrete Structure (GB50010-2010). The stress-strain curve is shown in Figure 3. The uniaxial tensile stress-strain curve equation of concrete is

$$\sigma = (1 - d_t) E_c \varepsilon, \quad (2)$$

$$d_t = \begin{cases} 1 - \rho_t [1.2 - 0.2x^5] & x \leq 1 \\ 1 - \frac{\rho_t}{\alpha_t (x - 1)^{1.7} + x} & x > 1, \end{cases}$$

$$x = \frac{\varepsilon}{\varepsilon_t},$$

$$\rho_t = \frac{f_t^*}{E_c \varepsilon_t},$$

where  $\alpha_t$  is the parameter value of curve falling section, obtained according to the specification of different concrete strength;  $f_t^*$  is the uniaxial tensile strength of concrete

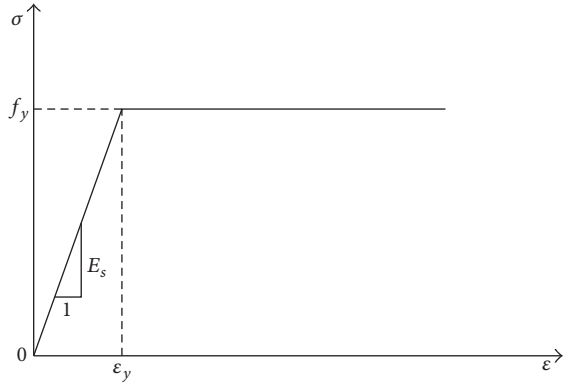


FIGURE 4: Perfectly plastic model.

obtained by material test;  $\varepsilon_t$  is the peak tensile strain corresponding to  $f_t^*$ , the uniaxial tensile strength of concrete;  $d_t$  is the uniaxial tensile damage evolution coefficient of concrete.

Uniaxial compressive stress-strain curve equation of concrete is

$$\begin{aligned} \sigma &= (1 - d_c) E_c \varepsilon, \\ d_c &= \begin{cases} 1 - \frac{\rho_c n}{n - 1 + x^2} & x \leq 1 \\ 1 - \frac{\rho_c}{\alpha_c (x - 1)^2 + x} & x > 1, \end{cases} \\ x &= \frac{\varepsilon}{\varepsilon_c}, \\ \rho_c &= \frac{f_c^*}{E_c \varepsilon_c}, \\ n &= \frac{E_c \varepsilon_c}{E_c \varepsilon_c - f_c^*}, \end{aligned} \quad (3)$$

where  $\alpha_c$  is the parameter value of curve falling section, obtained according to the specification of different concrete strength;  $f_c^*$  is the uniaxial compressive strength of concrete obtained by material test;  $\varepsilon_c$  is the peak tensile strain corresponding to  $f_c^*$ , the uniaxial compressive strength of concrete;  $d_c$  is the uniaxial compression damage evolution coefficient of concrete;  $E_c$  is the elastic modulus of the concrete.

In the finite element model, the constitutive relationship of H-steel, ordinary steel, and prestressing tendon is perfectly plastic model, which is shown in Figure 4.

**2.5. Element Types and Boundary Conditions.** ABAQUS offers a variety of elements; the literature [12], using the ‘‘Euler-Bernoulli’’ beam elements and ‘‘Timoshenko’’ beam elements to simulate concrete beam and using keyword Rebar to simulate the nonprestressed steel, but using beam element to simulate the prestressed concrete beam, is an approximate simulation method; there are still shortcomings. In this paper, solid element C3D8R was used to stimulate the concrete; Truss element T3D2 is the linear component which can only withstand tensile and compressive loads in

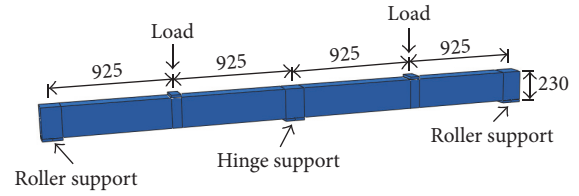


FIGURE 5: Two-span PSRC beam finite element model.

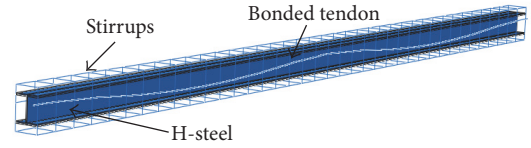


FIGURE 6: Steel and H-steel finite element model.

space, which is used to simulate nonprestressed steel and prestressed steel; H-steel girder was modeled by using four-node reduced-integration shell element S4R, which allows shear deformation change with the thickness varying in the thickness direction, its solving method will automatically obey the thick shell theory or shell theory. S4R is finite strain shell element considering the finite membrane strains and rotation is suitable for large strain analysis [13]. Simple support conditions simulating hinge and roller supports were applied to the ends of the beam. The finite element model is shown in Figures 5 and 6.

There are two load steps in the model; the first step only counts the response of beam under the effective prestressed force and its own weight; the second step is gradually applying displacement on the mid of the beam span. In order to prevent the stress concentration from appearing at the bottom of the beam in the loading process, steel pads were applied on the beam. Before applying the vertical displacement, the translational degrees of freedom on the vertical load direction of all nodes on the surface of loading surface were coupled. Considering geometric nonlinear effects the analysis step used ‘‘Static General’’ algorithm.

### 3. Comparative Analysis of Finite Element Results

After calculation, load-deflection curves of the mid-span of PSRC beam obtained from FE analysis and experimental results are compared in Figure 7.

Figure 7 shows that the maximum capacity of beam ( $f_u$ ) in finite element model is slightly larger than the experimental values. The more results can be calculated by using the energy equivalent method [13]; the yield load ( $f_y$ ) of experimental beam and finite element model is 234.10 kN and 245.52 kN, respectively, the difference value of which is 4.87%; the yield displacement experimental beam is 6.58 mm, the yield displacement of finite element model is 6.86 mm, the difference value is 4.26%, and both error values are controlled within 5%. The stiffness and bearing capacity differences between the finite element simulations with the

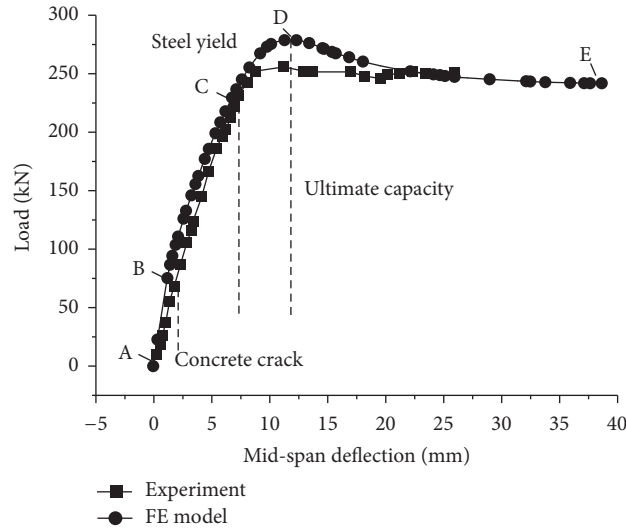


FIGURE 7: Finite element analysis result and experimental result.

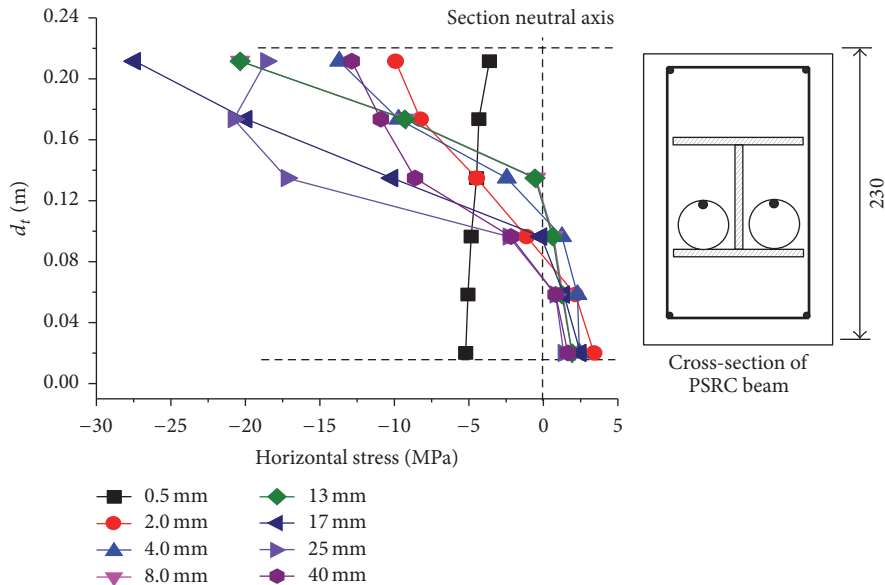


FIGURE 8: Mid-span section stress.

experimental results are mainly caused by the model not considering the bond slipping between steel and concrete, general program limitations, and other factors. Furthermore, the load-deflection curve in Figure 7 can be divided into four sections, A-B is before concrete cracked, B-C is from the concrete cracked to the tensile nonprestressed steel, H-steel yield, C-D is from the steel yielded to reaching the ultimate capacity, and D-E represents the plastic deformation stage.

#### 4. Section Stiffness and Stress Analysis of PSRC Beam

Beam deflection consists of three parts: first, the deflection of the beam generated by its own weight; second, inverted-arch deflection due to prestressed force; third, the deflection

caused by the load. In order to investigate the change of cross-section neutral axis and the section stiffness components in the loading process, the horizontal stress results of a series of points across the beam cross-section under different loading displacement were extracted. Figure 8 shows the horizontal stress of a series of nodes on the mid-span section under different displacements (0.5 mm, 2.0 mm, 4.0 mm, 8.0 mm, 13 mm, 17 mm, 25 mm, and 40 mm), in which  $d_t$  represents the distance from the nodes to the beam bottom.

As Figure 8 shows, PSRC beam deformation can be also broadly divided into four stages.

*First Stage.* At this point load displacement is small, the compressive stress generated by prestressed force is not offset. As a result, the stress of entire cross-section is compressive stress,

and affected by the prestressed force the neutral axis position moved down under the previous stage loading.

*Second Stage.* With the load displacement increasing, the concrete at the bottom of the mid-span section begins to bear tensile stress; however, because the load displacement is smaller, the concrete at the section bottom does not reach the ultimate tensile strength, so there is no crack in the entire section, and the section stiffness can be regarded as the stiffness consisting of prestressed concrete and H-steel.

*Third Stage.* With the load displacement increasing, the concrete at the section bottom cracked and gradually stopped bearing tension force; the figure shows that when the deflection increases from 4.0 mm to 13 mm, the neutral axis constantly moves; at this stage the beam section stiffness consists of confined concrete core, perimeter concrete (including tendons conversion section), and H-steel stiffness.

*Fourth Stage.* The bottom flange of H-steel will be yielded with the increase of the loading deflection, which results in the decrease of the section stiffness and the gradual rise of neutral axis. As can be seen from the figure, when the deflection increases from 13 mm to 25 mm, the distance between the neutral axis and beam bottom increases from 0.13 m to 0.18 m. At this point, the beam section stiffness consists of confined concrete core, a part of surrounding concrete, and H-steel stiffness. In addition, with the loading displacement increasing before the concrete on the top of the beam is crushed, the neutral axis position no longer moves up.

## 5. Comparative Analysis of PSRC Beam Capacity

In this section, in order to investigate the effect of prestress on the yield strength, ultimate strength and ductility of RC (reinforced concrete) beam, SRC (steel reinforced concrete) beam, and the changes of mechanical properties of beam after built-in H-steel, four same size numerical models were made, which are prestressed steel reinforced concrete (PSRC) beams, steel reinforced concrete (SRC) beams, prestressed reinforced concrete (PRC) beams, and reinforced concrete (RC) beams, and their mechanical properties were analyzed.

It can be seen from Figure 9 that the load-mid-span deflection curves of SRC beam generally have a twofold feature, which is different from the three-line feature of RC beam; it shows that the SRC beam has relatively high capacity. Compared with the PRC beam, the ultimate bearing capacities of the SRC beam and PSRC beam increase with the addition of internal H-steel, and the SRC beam and PSRC beam still have high bearing capacity in the plastic stage; however, the bearing capacity of PRC beam after the ultimate load decreases sharply. Compared with SRC beam, there is inverted-arch deflection before loading in PSRC beam, and the cracking load is improved, so the cracking load of PSRC beam is 68 kN; the cracking load of SRC is only 26 kN; it can be confirmed that the prestressed force can improve load carrying capacity of the beam under service load conditions.

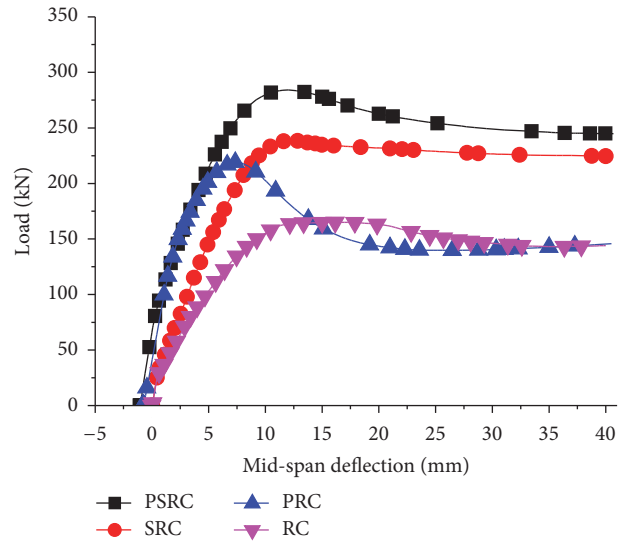


FIGURE 9: Load-mid-span deflection curves.

Ductility is an important index to reflect the deformation and energy dissipation of composite beams; in this paper, the displacement ductility coefficient  $\beta_{\Delta}$  is used to evaluate the ductility of the beam, the calculation formula of which is as follows:

$$\beta_{\Delta} = \frac{\Delta_u}{\Delta_y}. \quad (4)$$

It can be seen from Table 1 that, compared with the PRC beam, the ductility and capacity of the PSRC beam have been significantly increased, the ductility increased by 56.49%, and the ultimate capacity increased by 35.89%; being affected by the built-in H-steel, the improvement of the ductility was more obvious; moreover, the comparison of PRC beam and RC beam shows that adding prestressed steel increases the cracking load and section stiffness of beam, but ductility deteriorated. It is clear that prestressed steel can increase the bearing capacity of beam under normal use state, but the ductility of the beam may be reduced.

## 6. Conclusion

- (1) Using ABAQUS finite element model can accurately simulate the stress and deformation of experiment components; under the premise of rational boundary conditions and accurate material constitutive relations, the results have higher credibility.
- (2) Load-mid-span deflection curves of SRC beam generally have a twofold feature, which is different from the three-line feature of RC beam. The bearing capacities of PSRC beam and SRC beam keep at a high level; even at the plastic stage, it can be seen that PSRC beam and SRC beam have higher capacity and ductility.
- (3) PSRC beam has inverted-arch deflection before loading, which was advantageous to the normal use

TABLE 1: The table of load, displacement, and ductility of beams.

Beam classification	$\Delta_y$ (mm)	$f_y$ (kN)	$\Delta_u$ (mm)	$f_u$ (kN)	$\beta_\Delta$
PSRC	6.86	245.52	12.02	284.19	2.05
SRC	7.70	216.40	12.28	238.73	1.83
PRC	6.70	181.50	7.44	209.14	1.31
RC	8.49	144.10	11.46	164.10	1.53

of beam. Compared with SRC beam, PSRC beam cracks latter and has larger section stiffness and good deformation recovery performance.

- (4) The prestress can improve the crack resistance of the beam but reduce the ductility. Adding H-steel can improve the ductility and ultimate strength of beam; furthermore, the increase of ductility is more significant.

### Conflicts of Interest

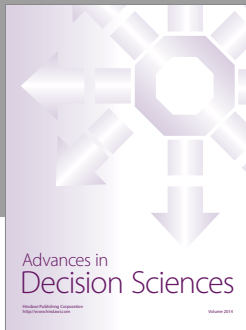
The authors declare that they have no conflicts of interest.

### Acknowledgments

The authors gratefully acknowledge the supports from the Program for Natural Science Foundation of Zhejiang Province (LY16E080006) and the Program for Science and Technology Foundation of Guangzhou City (201704020148).

### References

- [1] G. Manfredi, G. Fabbrocino, and E. Cosenza, "Modeling of steel-concrete composite beams under negative bending," *Journal of Engineering Mechanics*, vol. 125, no. 6, pp. 654–662, 1999.
- [2] H. Xiao, A. Li, and D. Du, "Experimental study on ultimate flexural capacity of steel encased concrete composite beams," *Journal of Southeast University (English Edition)*, vol. 21, no. 2, pp. 191–196, 2005.
- [3] C. Fu, Y. Li, X. Sun, and J. Xu, "Experimental study on seismic performance of prestressed and non-prestressed steel reinforced concrete frames," *Journal of Building Structures*, vol. 31, no. 8, pp. 15–21, 2010.
- [4] A. Zona and G. Ranzi, "Finite element models for nonlinear analysis of steelconcrete composite beams with partial interaction in combined bending and shear," *Finite Elements in Analysis and Design*, vol. 47, no. 2, pp. 98–118, 2011.
- [5] N. Zhang and C. C. Fu, "Experimental and theoretical studies on composite steel-concrete box beams with external tendons," *Engineering Structures*, vol. 31, no. 2, pp. 275–283, 2009.
- [6] Z. Chen, X. Fu, X. Yang, S. Chen, and L. Gu, "Study on steel reinforced concrete Vierendeel portal structure—portal structure design of Shenzhen University Science and Technology Building," *Journal of Building Structures*, vol. 25, no. 2, pp. 64–71, 2004.
- [7] X. Hu and W. Xue, "Progress in research and application of PSRC beams," *Architecture Technology*, vol. 37, no. 5, pp. 336–339, 2006.
- [8] P. Fanning, "Nonlinear models of reinforced and post-tensioned concrete beams," *Electronic Journal of Structural Engineering*, vol. 1, no. 2, pp. 111–119, 2001.
- [9] Z. Wenzhong, J. Wang, B. Han, H. Ye, and Y. Zhang, "Experimental research on mechanical behavior of continuous prestressed composite concrete beams with encased H-steel," *Journal of Building Structure*, vol. 31, no. 7, pp. 23–31, 2010.
- [10] K. Chen, J. Song, and S. Zhang, "Simulation and analysis for externally prestressed concrete bridge based on ANSYS," *Advanced Materials Research*, vol. 243, pp. 1737–1742, 2011.
- [11] K. Baskar, "Finite-element analysis of steel-concrete composite plate girder," *Journal of Structural Engineering*, vol. 128, no. 9, pp. 1158–1168, 2002.
- [12] ABAQUS, *Abaqus Analysis User's Manual-Version 6.8*, ABAQUS, 2008.
- [13] M. Murthy, D. R. Mahapatra, K. Badarinarayana et al., "A refined higher order finite element for asymmetric composite beams," *Composite Structures*, vol. 67, no. 1, pp. 27–35, 2005.



# Hindawi

Submit your manuscripts at  
<https://www.hindawi.com>

